



1 **Vertical changes in volatile organic compounds (VOCs) and**  
2 **impacts on photochemical ozone formation**

3 Xiao-Bing Li<sup>1</sup>, Bin Yuan<sup>1,\*</sup>, Yibo Huang<sup>1</sup>, Suxia Yang<sup>2</sup>, Xin Song<sup>1</sup>, Jipeng Qi<sup>1</sup>,  
4 Xianjun He<sup>1</sup>, Sihang Wang<sup>1</sup>, Yubin Chen<sup>1</sup>, Qing Yang<sup>1</sup>, Yongxin Song<sup>1</sup>, Yuwen Peng<sup>1</sup>,  
5 Guiqian Tang<sup>3,4</sup>, Jian Gao<sup>5</sup>, Min Shao<sup>1</sup>

6 <sup>1</sup> College of Environment and Climate, Institute for Environmental and Climate  
7 Research, Guangdong-Hongkong-Macau Joint Laboratory of Collaborative Innovation  
8 for Environmental Quality, Jinan University, Guangzhou 511443, China

9 <sup>2</sup> Guangzhou Research Institute of Environment Protection Co., Ltd., Guangzhou  
10 510620, China

11 <sup>3</sup> State Key Laboratory of Atmospheric Environment and Extreme Meteorology,  
12 Institute of Atmospheric Physics, Chinese Academy of Sciences, Beijing 100029, China

13 <sup>4</sup> University of Chinese Academy of Sciences, Beijing, 100049, China

14 <sup>5</sup> State Key Laboratory of Environmental Criteria and Risk Assessment, Chinese  
15 Research Academy of Environmental Sciences, Beijing 100012, China

16 \* Corresponding author: Bin Yuan ([byuan@jnu.edu.cn](mailto:byuan@jnu.edu.cn))



## 17 **Abstract**

18 Volatile organic compounds (VOCs) play crucial roles in regulating the formation  
19 of tropospheric ozone. However, limited knowledge on the interactions between  
20 vertical VOC variations and photochemical ozone formation has hindered effective  
21 ozone control strategies, especially in large cities. In this study, we investigated the  
22 vertical changes in concentrations, compositions, and key driving factors of a large suite  
23 of VOCs using online gradient measurements taken from a 325 m tall tower in urban  
24 Beijing. We also analyzed the impact of these vertical VOC variations on  
25 photochemical ozone formation using box model simulations. Our results indicate that  
26 the vertical variations of various VOC species are strictly regulated by the diurnal  
27 evolution of the planetary boundary layer. During daytime, reactive hydrocarbons are  
28 rapidly oxidized as they mix upwards, leading to the formation of OVOCs. This process  
29 plays a more significant role in regulating photochemical ozone formation with  
30 increasing height. In the lower layer, the photochemical formation of ozone responds  
31 positively to changes in both NO<sub>x</sub> and VOCs. As a result, the production rate of ozone  
32 decreases with height due to significant reductions in the concentrations of both NO<sub>x</sub>  
33 and VOCs, but remains high in the middle and upper layers. The strong production of  
34 ozone aloft is primarily driven by high concentrations of OVOCs and hydroxyl radicals,  
35 which can act as an important source of ozone at ground level. Therefore, careful  
36 consideration should be given to the vertical variations in both photochemical ozone  
37 production rates and formation regimes in the whole boundary layer when developing  
38 regional ozone control strategies.



## 39 1 Introduction

40 Volatile organic compounds (VOCs) are crucial constituents of atmospheric  
41 chemicals (*Li et al., 2022c*) and play important roles in regulating the atmospheric  
42 oxidation capacity and contributing to the photochemical formation of tropospheric  
43 ozone (*Zhao et al., 2022; Yang et al., 2024b*). Ozone is a major air pollutant in urban  
44 environments, with increasing trends reported globally over recent decades (*Fleming et*  
45 *al., 2018; Cooper et al., 2020*), despite stringent measures to control its precursor  
46 emissions (*Wang et al., 2020b; Yeo and Kim, 2021; Li et al., 2022b; Perdignes et al.,*  
47 *2022*). As highlighted in previous studies, reducing emissions of reactive VOCs is key  
48 to controlling ozone pollution at present and in the foreseeable future (*Zhao et al., 2022;*  
49 *Wang et al., 2024*).

50 The primary prerequisite for effective regional ozone pollution control is the  
51 determination of the photochemical ozone formation regime (*Souri et al., 2020; Zhao*  
52 *et al., 2022*), which facilitates the development of reduction schemes for key precursor  
53 emissions (*Ou et al., 2016; Wang et al., 2019*). The main challenges in controlling  
54 ozone pollution stem from the complex compositions of its precursors (e.g., VOCs and  
55 NO<sub>x</sub>) in ambient air (*Guo et al., 2017; Wu et al., 2020; Li et al., 2022c*), as well as the  
56 complicated responses of photochemical ozone formation to changes in these  
57 precursors (*Shao et al., 2021; Perdignes et al., 2022*). Furthermore, the interactions  
58 between vertical variations of ozone precursors and ozone formation remain unclear  
59 (*Tang et al., 2017; Sun et al., 2018; Li et al., 2024*), adding to the complexity of ozone  
60 pollution control.

61 In most cases, the identification of key ozone precursors has been conducted using  
62 ground-level observations (*Qi et al., 2021; Lu et al., 2022*) or compiled source emission  
63 inventories (*Ou et al., 2015; An et al., 2021; Wang et al., 2022b*). While these methods  
64 are undoubtedly helpful in determining key ozone precursors and corresponding  
65 reduction strategies, they often encounter unexpected uncertainties in urban regions.  
66 (*Mo et al., 2018; Mo et al., 2020*). Consequently, ground-level measurements of ozone



67 precursors have been favored to constrain model calculations (*Lu et al., 2012; Wang et*  
68 *al., 2022a; Yang et al., 2022*) or provide empirical evidence for hypothesized theories  
69 (*Hofzumahaus et al., 2009; Wang et al., 2022c*). However, these ground-level  
70 measurements cannot fully characterize atmospheric chemical processes in the entire  
71 planetary boundary layer (PBL) due to strong vertical variations in precursor  
72 concentrations (*Velasco et al., 2008; Li et al., 2018; Sun et al., 2018*).

73 Ambient VOCs, as crucial ozone precursors, are composed of myriad species (*Wu*  
74 *et al., 2020; Gkatzelis et al., 2021; Ye et al., 2021; He et al., 2022*) and serve diverse  
75 functions in photochemical ozone formation (*Vo et al., 2018; Li et al., 2022a; Zhang et*  
76 *al., 2022*). Owing to the impact of variations in emission sources, chemical removal,  
77 advection and convection transport, and secondary formation, the concentration and  
78 composition of VOCs typically display notable vertical variability within the PBL,  
79 especially in urban areas (*Li et al., 2022c*). The ozone formation regime like undergoes  
80 significant transitions from the ground to the upper boundary layer (*Li et al., 2024; Liu*  
81 *et al., 2024a*). Ozone generated throughout the PBL can influence surface ozone levels  
82 due to enhanced atmospheric vertical mixing during the day. Consequently, it is  
83 imperative to comprehend the vertical variations and principal determinants of VOCs,  
84 as well as their effects on photochemical ozone formation within the PBL.

85 With the rapid development of cities in the recent two decades in China, a large  
86 number of pollution-emitting industries and factories have been relocated from city  
87 centers to alleviate air pollution. Concurrently, there's been a swift increase in the  
88 ownership of electric vehicles (*Guo et al., 2021*). These shifts in energy consumption  
89 have driven the change in concentrations and compositions of VOCs in major cities like  
90 Beijing (*Liu et al., 2024b*), subsequently affecting photochemical ozone formation  
91 (*Wang et al., 2024*). However, the vertical variations and key drivers of VOCs and their  
92 impacts on photochemical ozone formation in the urban PBL remain elusive. A primary  
93 hurdle in studying these vertical changes in photochemical ozone formation is the  
94 scarcity of reliable vertical VOC data (*Dieu Hien et al., 2019; Li et al., 2022c*).  
95 Engaging in vertical profiling of VOCs, ensuring all necessary species represented and



96 obtaining sufficient sample size, is especially challenging in the lower PBL where  
97 atmospheric chemical reactions are most intense (*Benish et al., 2020; Kim et al., 2021*).

98 Previous studies on vertical distributions of photochemical ozone formation in the  
99 PBL have been conducted using measurements of a limited number of VOC species  
100 and samples (*Zhang et al., 2018; Benish et al., 2020; Geng et al., 2020*). In this study,  
101 online gradient measurements of ozone, NO<sub>x</sub>, and a large suit of VOCs were made on  
102 a 325 m tall tower in urban Beijing during the summer of 2021. Additionally, box model  
103 simulations constrained by the gradient measurements were performed to analyze the  
104 vertical variations and key drivers of VOCs as well as their impacts on photochemical  
105 ozone formation.

## 106 **2 Methods and materials**

### 107 **2.1 Description of the site, instrument, and field campaign**

108 The data utilized in this study was derived from an intensive field campaign  
109 conducted at the Beijing Meteorological Tower (BMT: 39°58' N, 116°23' E) between  
110 July 6 and August 4, 2021. The BMT has a height of 325 m and is located in the northern  
111 part of downtown Beijing, positioned between the third and fourth ring roads (Fig. S1).  
112 A vertical observation system, established using long perfluoroalkoxy alkane (PFA)  
113 Teflon tubes (OD: 1/2 in.), was used to make online gradient measurements of ozone,  
114 NO<sub>x</sub>, and a set of VOCs on the BMT. Five specific heights, namely 15, 47, 102, 200,  
115 and 320 m above ground level, were selected to mount the tube inlets, as depicted in  
116 Fig. S2. An additional inlet, situated approximately 5 m above ground level, was  
117 mounted on the rooftop of the observation room that was adjacent to the tower.  
118 Consequently, the vertical observation system totally included a total of six sampling  
119 inlets. The sampling inlet at the 15 m height was not utilized during this field campaign.

120 Filters were installed downstream of the tubing inlets on the tower to remove fine  
121 particles. A rotary vane vacuum pump was used to simultaneously and continuously  
122 draw sample air from the five tubes, ensuring that all tubes were flushed by ambient air



123 to reduce tubing delays of sticky organic compounds (Pagonis *et al.*, 2017; Liu *et al.*,  
124 2019). Five critical orifices were employed to control the flow rate of the air stream in  
125 each tubing, resulting in flow rates ranging between 15 and 20 standard liter per minute  
126 (SLPM). Instruments drew sample air from the five tubes sequentially through a Teflon  
127 solenoid valve group at designated time intervals. The switching time intervals of the  
128 Teflon solenoid valve group were set as 4 minutes during this field campaign. The  
129 measurements of trace gases in the first and last 1 minute of a four-minute period were  
130 discarded to eliminate cross interferences between different inlet heights. Detailed  
131 information on the vertical observation system and the assessment of trace gas  
132 measurements through hundreds of meters long PFA tubes has been provided in our  
133 previous works (Li *et al.*, 2023; Yang *et al.*, 2024a).

134 Ozone was measured using the ultraviolet photometry method (49i, Thermo Fisher  
135 Scientific Inc., USA). NO, NO<sub>2</sub>, and NO<sub>x</sub> were measured using the chemiluminescence  
136 method (42i, Thermo Fisher Scientific Inc., USA). Gradient measurements of ozone  
137 and NO<sub>x</sub> were conducted at a time resolution of 10 seconds. The photolysis frequencies  
138 of NO<sub>2</sub>, represented by  $j(\text{NO}_2)$ , were measured by a spectrometer (PFS-100, Focused  
139 Photonics Inc., China) situated on the rooftop of the observation room and have a time  
140 resolution of 8 seconds. In situ measurements of meteorological parameters including  
141 wind speed, air temperature, and relative humidity were made at 15 heights between 8  
142 m and 320 m on the BMT with a time resolution of 20 seconds. Planetary boundary  
143 layer height (PBLH) was obtained from the Air Resources Laboratory  
144 (<https://ready.arl.noaa.gov/READYamet.php>, last access: 10 June 2024) and was  
145 linearly interpolated to hourly values based on the initial time resolutions of three hours  
146 (Li and Fan, 2022).

147 A high-resolution proton-transfer-reaction quadrupole interface time-of-flight  
148 mass spectrometer (PTR-ToF-MS, Ionicon Analytik, Austria) was employed to measure  
149 VOCs at a time resolution of 10 seconds. The PTR-ToF-MS used both hydronium ion  
150 ( $\text{H}_3\text{O}^+$ ) (Yuan *et al.*, 2017; Wu *et al.*, 2020; Li *et al.*, 2022c) and nitric oxide ion ( $\text{NO}^+$ )  
151 (Wang *et al.*, 2020a) as reagent ions. These two reagent ions were automatically



152 switched every 60 min for  $\text{H}_3\text{O}^+$  and every 22 min for  $\text{NO}^+$  throughout the campaign.  
153 The PTR-ToF-MS operated at an E/N value of approximately 120 Td in  $\text{H}_3\text{O}^+$  mode  
154 and an E/N value of around 60 Td in  $\text{NO}^+$  mode. Instrument backgrounds were  
155 automatically measured during the last two minutes of each operation mode by passing  
156 ambient air through a platinum catalyst heated to 365 °C. A gas standard containing 39  
157 VOC species was used to calibrate the PTR-ToF-MS daily. Sensitivities for the  
158 remaining species were determined based on reaction kinetics of the PTR-ToF-MS (*Wu*  
159 *et al.*, 2020). Impacts of ambient humidity on the PTR-ToF-MS measurements were  
160 corrected by using humidity-dependence curves of VOCs obtained in our laboratory  
161 (*Wang et al.*, 2020a; *Wu et al.*, 2020). Carbon dioxide ( $\text{CO}_2$  in dry air) and humidity  
162 were measured using a  $\text{CO}_2$  and  $\text{H}_2\text{O}$  gas analyzer (Li-840A, Licor Inc., USA) at a time  
163 resolution of 10 seconds.

164 Gradient measurements of the total OH reactivity (OHR) of atmospheric trace  
165 gases were made using the improved comparative reactivity method (ICRM) developed  
166 by our team (*Wang et al.*, 2021a) from July 28 to 31. In addition, gradient measurements  
167 of carbon monoxide (CO), methane ( $\text{CH}_4$ ),  $\text{CO}_2$ , and  $\text{H}_2\text{O}$  were simultaneously  
168 measured using the cavity ring-down spectroscopy (CRDS) method (G-2401, Picarro  
169 Inc., USA) at a time resolution of 10 seconds from May 15 to June 25. Sulfur dioxide  
170 ( $\text{SO}_2$ ) was measured using the ultraviolet fluorescence method (43i, Thermo Fisher  
171 Scientific Inc., USA) at a time resolution of 10 seconds from June 25 to August 3. The  
172 total OHR of VOCs, denoted by  $\text{OHR}_{\text{VOCs}}$ , can be estimated by excluding those of the  
173 inorganic species (namely ozone,  $\text{NO}_x$ , CO,  $\text{SO}_2$ , and  $\text{CH}_4$ ). It should be noted that  
174 gradient measurements of  $\text{CH}_4$  and CO were not made during July 28-31, and their  
175 average concentrations in daytime (11:00-16:00 LT) between May 15 and June 25 at 5  
176 m were used for all altitudes to calculate  $\text{OHR}_{\text{VOCs}}$ . This method will bring minor  
177 uncertainties due to the minor vertical differences in concentrations of  $\text{CH}_4$  and CO in  
178 daytime (Fig. S3). The OHR of VOCs can also be calculated by summing the products  
179 of their measured concentrations and their reaction rate coefficients with OH radicals,  
180 as formulated in Eq. (1):



$$\text{OHR} = \sum k^i_{\text{OH-R}}[\text{VOC}_i] \quad \text{Eq. (1)}$$

181 where  $k^i_{\text{OH-R}}$  is the reaction rate coefficient of the  $i^{\text{th}}$  VOC species with OH radical  
 182 and  $[\text{VOC}_i]$  is the concentration of the  $i^{\text{th}}$  VOC species.

## 183 2.2 Estimation of NMHC concentrations at the BMT site

184 The PTR-ToF-MS is limited in its ability to measure VOC species with proton  
 185 affinities higher than  $\text{H}_2\text{O}$  ( $691 \text{ kJ mol}^{-1}$ ) when operating in the  $\text{H}_3\text{O}^+$  mode (*Yuan et*  
 186 *al., 2017*). This limitation results in the absence of certain nonmethane hydrocarbons  
 187 (NMHCs), such as alkanes and many alkene species, which play important roles in  
 188 photochemical ozone formation. To obtain a comprehensive understanding of vertical  
 189 variations in concentrations, compositions, and environmental impacts of VOCs, this  
 190 study estimated the vertical profiles of those unmeasured NMHC species based on the  
 191 concentrations of measured VOCs using the PTR-ToF-MS. Detailed information on  
 192 estimation of NMHC concentrations is provided in SI.

## 193 2.3 Box model setup

194 A zero-dimension box model (F0AM) coupled with the Master Chemical  
 195 Mechanism (v3.3.1) (*Wolfe et al., 2016; Yang et al., 2022*) was used to compute the  
 196 production rate of ozone, denoted by  $\text{P}(\text{O}_3)$  as formulated in Eq. (2):

$$\text{P}(\text{O}_3) = k_{\text{HO}_2+\text{NO}}[\text{HO}_2][\text{NO}] + \sum k^i_{\text{RO}_2+\text{NO}}[\text{R}^i\text{O}_2][\text{NO}] \quad \text{Eq. (2)}$$

$$k_{\text{RO}_2+\text{NO}}[\text{RO}_2][\text{NO}]$$

198 where  $[\text{HO}_2]$  and  $[\text{NO}]$  is the concentrations of  $\text{HO}_2$  and  $\text{NO}$ ,  $[\text{R}^i\text{O}_2]$  is the concentration  
 199 of the  $i^{\text{th}}$  organic peroxy radical. The relative incremental reactivity (RIR) of  
 200 photochemical ozone production to changes in different precursors was determined  
 201 using Eq. (3):

$$\text{RIR}(X) = \frac{[P_{\text{O}_3}^S(X) - P_{\text{O}_3}^S(X - \Delta X)]/P_{\text{O}_3}^S(X)}{\Delta S(X)/S(X)} \quad \text{Eq. (3)}$$





202 where X represents ozone precursors,  $P_{O_x}^S(X)$  is the contribution of X to the production  
203 rate of  $O_x$ ,  $\Delta X$  is the amount of change in ozone precursors,  $S(X)$  is the initial  
204 concentration of X. RIR values were used to discern sensitivities of photochemical  
205 ozone formation to changes in precursor gases. A positive RIR(X) value suggests that  
206 an increase in X enhances ozone formation, while a negative RIR value indicates that  
207 an increase in X inhibits ozone formation.

208 Model calculations were constrained by measurements of ozone,  $NO_x$ , CO, a suit  
209 of VOCs, air temperature, and relative humidity. In addition to the measured or  
210 estimated concentrations of NMHCs, nine oxygenated VOC (OVOC) species (Table  
211 S1) measured by PTR-ToF-MS were used to constrain the model calculation. The  
212 model was run in a time-dependent mode with a time resolution of 5 minutes and a  
213 spin-up period of 2 days (Lu *et al.*, 2012; Wang *et al.*, 2022c). The dry deposition  
214 velocity of ozone was set as  $0.27 \text{ cm s}^{-1}$  when calculating  $P(O_3)$  5 m and was zeroed  
215 out when calculating  $P(O_3)$  at other heights.

## 216 **3 Results and discussions**

### 217 **3.1 Temporal and vertical variations in concentrations of trace gases**

218 As shown in Fig. 1, the meteorology in Beijing was characterized by high air  
219 temperature ( $27.3 \pm 2.9 \text{ }^\circ\text{C}$ ), high humidity ( $83.9\% \pm 16.2\%$ ), and gentle winds ( $1.1 \pm 0.4$   
220  $\text{m s}^{-1}$ ) throughout the campaign. The intense solar radiation, elevated air temperature,  
221 and mild winds favored the photochemical formation and accumulation of ozone,  
222 leading to frequent occurrences of ozone pollution episodes. Fig. 1 also presents time  
223 series of mixing ratios of ozone and its selected precursors (namely isoprene, toluene,  
224 monoterpenes, and  $NO_x$ ) along with  $j(NO_2)$  measured at 5 m. The campaign mean  
225 ozone mixing ratio was  $45.6 \pm 25.3 \text{ ppb}$ , but the maximum hourly mean ozone mixing  
226 ratio reached  $129.3 \text{ ppb}$ , indicating strong photochemical reactions in urban Beijing  
227 during the campaign. Surface ozone concentrations exhibited a typical diurnal variation



228 pattern with the maximum occurring at 16:00 LT (Fig. S5), implying its predominant  
229 source from local photochemical production.

230 Isoprene is a typical tracer of biogenic emissions and is also a highly reactive VOC  
231 species (*Atkinson and Arey, 2003*). Isoprene had a campaign mean mixing ratio of  
232  $0.7\pm 0.6$  ppb. The average diurnal profile of isoprene at 5 m has a unimodal pattern with  
233 the maximum occurring at 14:00 LT (Fig. S5), exhibiting strong dependence on solar  
234 radiation. Monoterpenes were also generally recognized as typical tracers of biogenic  
235 emissions (*Gómez et al., 2020*) and have a campaign mean mixing ratio of  $0.3\pm 0.3$  ppb.  
236 The average diurnal profile of monoterpenes was characterized by low mixing ratios in  
237 daytime with two peaks occurring at 05:00 and 20:00 LT, respectively.

238 Toluene and NO<sub>x</sub> are recognized as typical tracers of anthropogenic emissions in  
239 urban regions (*Niu et al., 2017; Li et al., 2022c*), with campaign mean mixing ratios of  
240  $0.7\pm 0.7$  and  $8.1\pm 4.8$  ppb, respectively. The average diurnal profiles of toluene and NO<sub>x</sub>  
241 at 5 m exhibited similar variations with larger values at night than during the day. Based  
242 on the measured concentrations and diurnal variations of ozone and its key precursors  
243 at ground level, it can be inferred that urban Beijing is experiencing severe ozone  
244 pollution, which is predominantly contributed by local photochemical production. As  
245 key ozone precursors, ambient concentrations of VOCs are contributed by the mixture  
246 of anthropogenic and biogenic sources.

247 Fig. 2 shows the average diurnal and vertical variations in mixing ratios of ozone,  
248 NO<sub>x</sub>, Ox (O<sub>3</sub>+NO<sub>2</sub>), and six selected VOC species (three hydrocarbons and three  
249 OVOCs) within the measurement height range of 5-320 m. High mixing ratios of ozone  
250 were observed in the afternoon following the enhancement of solar radiation, which  
251 was consistent with the diurnal change pattern of ozone concentrations at the ground  
252 level. The vertical gradients of ozone mixing ratios were positive throughout the day  
253 but substantially enhanced at night (Fig. 3). The lower ozone mixing ratios near the  
254 surface than aloft were mainly caused by the enhancement of dry deposition and NO  
255 titration (*Brown et al., 2007; Ma et al., 2013; Li et al., 2022b*).



256 NO<sub>x</sub> is a primary pollutant and mainly contributed by vehicular exhausts in urban  
257 regions. In contrast to ozone, NO<sub>x</sub> mixing ratios were low in daytime and exhibited  
258 negative vertical gradients throughout the day, as shown in Figs. 2B and 3A-B. In  
259 nighttime, large amounts of local NO<sub>x</sub> emissions were trapped and accumulated in a  
260 shallow boundary layer (<100 m). NO<sub>x</sub> concentrations rapidly decreased with height  
261 even in the overlying residual layer due to the suppression of turbulence vertical mixing.  
262 With the onset of sunlight, the PBL rapidly expanded due to the surface heating effect.  
263 The accumulated high concentrations of NO<sub>x</sub> in the shallow nocturnal boundary layer  
264 were thereupon diluted and removed by photochemical reactions.

265 Ox is frequently used as a conserved metric to investigate temporal and spatial  
266 variability of ozone by eliminating the NO titration effect. As shown in Fig. 2C, the  
267 mixing ratios of Ox had similar diurnal and vertical variation patterns to those of ozone,  
268 but the vertical gradients of Ox were weaker than those of ozone. This result suggests  
269 that the vertical distribution of NO concentrations played an important role in regulating  
270 the vertical change of ozone concentrations. The enhanced positive gradients of ozone  
271 mixing ratios at night were predominantly due to the strict suppression of turbulence  
272 vertical mixing (*Geyer and Stutz, 2004*). The higher concentrations of ozone aloft are  
273 considered as the residual of the ozone produced in the daytime PBL and have been  
274 recognized as an important reservoir for the enhancement of surface ozone in morning  
275 periods (*Kaser et al., 2017; Li and Fan, 2022; He et al., 2023*).

276 Benzene and toluene demonstrated similar diurnal and vertical variations to NO<sub>x</sub>,  
277 with low concentrations in daytime and high concentrations at night, as shown in Figs.  
278 2D-F and 3A-B. The concentrations of both benzene and toluene decreased with height  
279 throughout the day, confirming their primary emissions from ground-level sources.  
280 However, unlike benzene, the diurnal and vertical variations of toluene were more  
281 pronounced. Isoprene emissions are highly dependent on solar radiation, resulting in its  
282 higher concentrations in the early afternoon compared to other times of the day.  
283 Isoprene mixing ratios also exhibited strong negative vertical gradients below 320 m  
284 throughout the day. In contrast to toluene, isoprene concentrations decreased more



285 rapidly with height in the daytime. For instance, the mixing ratios of isoprene decreased  
286 by approximately 70% from 5 to 320 m in the daytime, while it was only 30% for  
287 toluene.

288 Fig. 3A-B show the average vertical profiles of the NMHCs, normalized to their  
289 respective ground-level concentrations measured by the PTR-ToF-MS in daytime and  
290 nighttime. The normalized mixing ratios of the NMHCs exhibited significantly  
291 differentiated gradients in daytime. In contrast, apart from monoterpenes, the  
292 differences in vertical gradients of the normalized vertical profiles for other NMHCs  
293 were relatively small at night. The differentiated vertical gradients of the NMHCs in  
294 daytime were primarily caused by their intrinsic chemical reactivities, such as reactions  
295 with OH radicals. As shown in Fig. 4, concentration ratios of the NMHC species  
296 between 320 m and 5 m with  $k_{OH}$  values lower than  $2.5 \times 10^{-11} \text{ cm}^{-3} \text{ molecule}^{-1} \text{ s}^{-1}$   
297 exhibited slight variability and rapidly declined with the further increases in  $k_{OH}$ . The  
298 lower NMHC concentrations at higher altitudes were predominantly caused by the  
299 combined effects of atmospheric diffusion and chemical removal (*Sangiorgi et al.*,  
300 2011).

301 Considering the effects of atmospheric diffusion and chemical removal by  
302 reactions with OH radicals, concentration ratios of NMHC species between 320 m and  
303 5 m in daytime can be estimated using Eq. (4):

$$y = A \times \exp(-k_{OH}[\text{OH}]\Delta t) \quad \text{Eq. (4)}$$

304 where  $y$  represents concentration ratios of the NMHC species between two altitudes,  $A$   
305 represents the effect of atmospheric dilution,  $k_{OH}$  is the reaction rate coefficient of  
306 NMHCs with OH radicals,  $[\text{OH}]$  is the concentration of OH radical,  $\Delta t$  is the  
307 turbulence mixing time scale between the two altitudes. The term  $[\text{OH}]\Delta t$  thus refers  
308 to the exposure of NMHCs to OH radicals between the two altitudes. As shown in Fig.  
309 4, the average concentration ratios of NMHCs between 320 m and 5 m in daytime  
310 during the campaign can be well reproduced using Eq. (4) with the coefficients  $A$  of  
311 0.88 and  $[\text{OH}]\Delta t$  of  $1.0 \times 10^{10} \text{ molecules cm}^{-3} \text{ s}$ . Atmospheric diffusion processes have  
312 same impact on the vertical distributions of all trace gases. The differences in vertical



313 gradients of NMHCs were mainly determined by the differences in their chemical  
314 removal rates without considering influences from advection transport.

315 Methanol, as one of the most abundant OVOC species in the atmosphere, had its  
316 lowest concentrations during daytime and displayed negative vertical gradients  
317 throughout the day, as shown in Fig. 2G. The vertical and diurnal variations of methanol  
318 suggest that its ambient concentrations in urban Beijing were mainly contributed by  
319 local primary emissions. Conversely, formaldehyde and MVK+MACR (the first-  
320 generation oxidation products of isoprene), as the photochemical oxidation products of  
321 NMHCs, had higher concentrations during daytime than at night and exhibited  
322 relatively weak vertical concentration gradients (Fig. 2H-I). This is mainly because  
323 these OVOCs are produced from the oxidation of NMHCs during turbulence vertical  
324 mixing and will accumulate in high altitudes. These phenomena were also observed for  
325 other OVOC species, as shown in Fig. 3.

326 The vertical and diurnal variations in concentrations of ozone, NO<sub>x</sub>, and VOCs  
327 are intricately governed by their sources, chemical reactivities, and the evolution of the  
328 PBL (namely the vertical dilution conditions). A significant accumulation of VOCs in  
329 the shallow nocturnal PBL is subsequently vertically diluted and chemically removed  
330 during daytime, thereby impacting the photochemical formation of ozone within the  
331 daytime PBL. In addition, the observed vertical changes in concentrations of VOCs  
332 imply that they will play distinct roles in contributing to photochemical ozone  
333 formation.

### 334 **3.2 Vertical variations in contributions of VOCs to OHR**

335 During the daytime, VOCs are primarily oxidized by OH radicals and contribute  
336 to the photochemical formation of ozone. To provide an overview on the vertical  
337 variations in contributions of different VOCs to OHR, another 1204 ions measured by  
338 the PTR-ToF-MS and can be quantified were used for analysis. All the VOCs were  
339 classified into three large categories, namely C<sub>x</sub>H<sub>y</sub> (including alkanes, alkenes,  
340 aromatics, and other hydrocarbons; 121 species), OVOCs (C<sub>x</sub>H<sub>y</sub>O<sub>1</sub>, 121 species;



341  $C_xH_yO_2$ , 120 species;  $C_xH_yO_{\geq 3}$ , 256 species), and N/S-containing (653 species), as  
342 shown in Fig.5. Acetylene is included in alkenes.

343 Fig. 5A illustrates that the total mixing ratios of VOCs in daytime exhibited a slight  
344 downward trend from 5 m to 320 m, primarily due to the rapid decrease in mixing ratios  
345 of the  $C_xH_y$  category. The total mixing ratios of the  $C_xH_y$  category decreased from 16.8  
346 to 10.6 ppb from 5 m to 320 m, with alkanes making the largest contribution, followed  
347 by alkenes, aromatics, and other  $C_xH_y$ . Alkanes constituted 58% of the total mixing  
348 ratios of  $C_xH_y$  at 5 m, but this proportion increased to 65% at 320 m. The fractional  
349 contributions of alkenes and aromatics in the total mixing ratios of  $C_xH_y$  slightly  
350 declined from 28% to 22% and from 12% to 10%, respectively, between these two  
351 altitudes. As for OVOCs, the  $C_xH_yO_1$  category was the most abundant among the  
352 measurements, contributing to 52%-58% of the total mixing ratios at the five heights,  
353 followed by the  $C_xH_yO_2$  (8%-10%), and  $C_xH_yO_{\geq 3}$  (2%) categories. The mixing ratios of  
354 the N/S-containing category slightly varied around 2.8 ppb between 5-320 m,  
355 contributed to approximately 6% of the total VOC concentrations.

356 Similar to the vertical variations in concentrations, OHRs of the  $C_xH_y$  category,  
357 denoted by  $OHR_{CH}$ , also rapidly decreased from  $6.9 s^{-1}$  to  $2.5 s^{-1}$  between 5 and 320 m,  
358 accounting for 52%-31% in the total OHRs of VOCs (Fig. 5B). Fractional contributions  
359 of alkenes (40-18%), alkanes (5%), and aromatics (5%-4%) to the total OHRs of VOCs  
360 all exhibited decreasing tendencies from 5 m to 320 m. The total OHRs of alkenes  
361 decreased more quickly from 5 to 320 m than those of alkanes and aromatics. OHRs of  
362 the other  $C_xH_y$  category stabilized at approximately  $0.3 s^{-1}$  below 320 m, exhibiting an  
363 increasing contribution (2%-4%) to the total OHRs of VOCs with the increase in height.  
364 The OHRs of other VOC categories only slightly varied without exhibiting a clear  
365 variation trend from 5 to 320 m during the day. As a result, fractional contributions of  
366 the  $C_xH_yO_1$  (27%-42%),  $C_xH_yO_2$  (12%-18%), and  $C_xH_yO_{\geq 3}$  (5%-7%), and N/S-  
367 containing (2%-4%) categories in the total OHRs of VOCs all increased with height.  
368 The increased contributions of OVOCs and N/S-containing species to the total



369 concentrations and OHRs of VOCs implied that air masses became more aged with the  
370 increase in height.

371 As depicted in Fig. 6A-B, high  $OHR_{CH}$  values were mainly constrained in the PBL  
372 and is mainly contributed by biogenic hydrocarbons, specifically isoprene, during  
373 daytime due to their high OH reactivities and enhanced emissions. The fractional  
374 contributions of isoprene in  $OHR_{CH}$  decreased rapidly with increasing height (Fig. 7A).  
375 For instance, isoprene accounted for a campaign median fraction of 58% in  $OHR_{CH}$  at  
376 5 m in daytime, making it a frequent contributor to photochemical ozone formation in  
377 urban regions. However, this fraction decreased to 38% at 320 m. Therefore, it can be  
378 speculated that the total contributions of hydrocarbons to the total OHRs of VOCs will  
379 also rapidly decline from 320 m to the top of the PBL, which typically ranges between  
380 several hundreds of meters to approximately 2~3 km in daytime (Fig. S6).

381 The total concentrations and OHRs of OVOCs only slightly decreased with the  
382 increase in height below 320 m in daytime, as shown in Fig. 6C-D. This is consistent  
383 with the results of (Wang *et al.*, 2021b), which observed high concentrations of OVOCs  
384 in the upper PBL. Consequently, the ratio of  $OHR_{OVOC}$  to  $OHR_{CH}$ , denoted by  
385  $OHR_{OVOC}/OHR_{CH}$ , rapidly increased from 0.87 at 5 m to 2.6 at 320 m (Fig. 7A). This  
386 suggests that OVOCs may play more important roles in regulating the photochemical  
387 ozone formation in the middle and upper layers. To assess their potential roles in  
388 contributing to the photochemical ozone formation throughout the PBL, we calculated  
389 the mean OHRs (MOHR) of different VOC categories in daytime using Eq. (5):

$$MOHR(X) = \left( \sum ([X]_i + [X]_{i-1})(h_i - h_{i-1})/2 \right) / (320 - 5) \quad \text{Eq. (5)}$$

390 where  $MOHR(X)$  is the MOHR of the VOC category X,  $[X]_i$  is the concentration of  
391 X at the  $i^{\text{th}}$  altitude (namely 5, 47, 102, 200, and 320 m for  $h_i$ ) above ground level.

392 As shown in Fig. 7B, the campaign median MOHR for isoprene was  $1.7 \text{ s}^{-1}$  and  
393 accounted for 48% of the campaign median MOHR of the  $C_xH_y$  category. This fraction  
394 was significantly lower than that of isoprene (57%) in  $OHR_{CH}$  at 5 m. In addition, the  
395 campaign median MOHR of the  $C_xH_y$  category ( $3.5 \text{ s}^{-1}$ ) was also significantly lower



396 than the  $\text{OHR}_{\text{CH}}$  ( $6.0 \text{ s}^{-1}$ ) at 5 m. By contrast, the campaign median MOHR of OVOCs  
397 ( $4.8 \text{ s}^{-1}$ ) was comparable to that of  $\text{OHR}_{\text{OVOC}}$  ( $4.9 \text{ s}^{-1}$ ) at 5 m. As unsaturated  
398 hydrocarbons, most alkene species are more reactive than alkanes and aromatics  
399 (*Atkinson and Arey, 2003*). As a result, alkenes had dominant contributions to the  
400 MOHR of the  $\text{C}_x\text{H}_y$  category and the  $\text{OHR}_{\text{CH}}$  at 5 m in daytime. As shown in Fig. 7C,  
401 the campaign mean OHRs of alkanes, alkenes, and aromatics at 5 m in daytime were  
402 0.7, 5.2, and  $0.7 \text{ s}^{-1}$ , respectively, accounting for 10%, 75%, and 10% of the  $\text{OHR}_{\text{CH}}$ .  
403 However, the campaign mean MOHRs of alkanes, alkenes, and aromatics were 0.5, 2.7,  
404 and  $0.5 \text{ s}^{-1}$ , respectively, accounting for 12%, 68%, and 12% of the MOHR of NMHC.  
405 We can also expect that the total contributions of alkenes to the MOHR of the  $\text{C}_x\text{H}_y$   
406 category in daytime will significantly decrease if their vertical distributions in the whole  
407 PBL are considered.

408 This study investigated and compared the vertical profiles of measured  $\text{OHR}_{\text{VOCs}}$   
409 and calculated  $\text{OHR}_{\text{CH}}$  during daytime over the period of July 28-31, as shown in Fig.  
410 7D. The campaign median of the measured  $\text{OHR}_{\text{VOCs}}$  exhibited a slow decrease from  
411  $38.4 \text{ s}^{-1}$  at 5 m to  $25.4 \text{ s}^{-1}$  at 320 m. As anticipated, the  $\text{OHR}_{\text{CH}}/\text{OHR}_{\text{VOCs}}$  ratio declined  
412 rapidly from 16% to 7% from 5 to 320 m. It is important to note that the small  
413  $\text{OHR}_{\text{CH}}/\text{OHR}_{\text{VOCs}}$  ratio and its declining trend with the increasing height do not imply  
414 the insignificant roles of hydrocarbons in regulating the secondary pollutant formation  
415 in higher altitudes. The measured concentrations of hydrocarbons are merely the  
416 remnants of chemical reactions. The oxidation products of NMHCs, such as OVOCs  
417 and organic nitrates, formed during vertical mixing in daytime, will continue to  
418 participate in atmospheric chemical reactions.

### 419 3.3 Vertical variations in photochemical ozone formation

420 The surface ozone budget is intimately linked to the vertical variations of  
421 photochemical ozone formation throughout the PBL. Previous studies have consistently  
422 reported that the photochemical formation of ozone, encompassing both  $\text{P}(\text{O}_3)$  and  
423 ozone formation regimes (namely the  $\text{NO}_x$ -limited, VOCs-limited, and transition





424 regimes), are highly dependent on the change in its precursors (*Shao et al., 2021; Yang*  
425 *et al., 2022*). Consequently, any changes in the concentrations and compositions of  
426 VOCs and NO<sub>x</sub> within the PBL will inevitably lead to alternations in the vertical  
427 distribution of P(O<sub>3</sub>) and ozone formation regimes (*Tang et al., 2017; Li et al., 2024*).

428 Fig. 8A illustrates the average dependence of P(O<sub>3</sub>) on NO<sub>x</sub> concentrations along  
429 with the normalized probability density (NPD) distribution of NO<sub>x</sub> concentrations at 5  
430 m, 200 m, and 320 m in daytime during the field campaign. At different heights, P(O<sub>3</sub>)  
431 all rapidly increased with the rise in NO<sub>x</sub> until a critical NO<sub>x</sub> mixing ratio was reached,  
432 after which P(O<sub>3</sub>) decreased slowly. The critical NO<sub>x</sub> mixing ratios decreased from  
433 approximately 9.5 ppb at 5 m to 5.0 m ppb at 320 m, primarily caused by the decreases  
434 in both NO<sub>x</sub> concentrations and the OHRs of VOCs. As also shown in Fig. 8A, the  
435 majority of the measured NO<sub>x</sub> mixing ratios fall into the transition zone of the P(O<sub>3</sub>)-  
436 NO<sub>x</sub> curves, suggesting that the photochemical ozone formation in Beijing belonged to  
437 the transition regime below 320 m.

438 RIR values were also calculated using the box model results to further elucidate  
439 the sensitivities of photochemical ozone formation to changes in multiple precursors at  
440 different altitudes. As shown in Fig. 8B, positive RIR values were observed for both  
441 NO<sub>x</sub> and various VOC groups at the five heights, further confirming that the  
442 photochemical ozone formation belonged to the transition regime in the lower layer.  
443 RIR values for NO<sub>x</sub> rapidly declined from 5 to 320 m, implying that the photochemical  
444 ozone formation in higher altitudes were more prone to be controlled by the abundance  
445 of VOCs. This is also manifested by the increasing RIR values for both AVOCs and  
446 OVOCs from 5 m to 320 m. RIR values for BVOCs significantly decreased with height  
447 due to their rapid removal by reactions with OH radicals when being vertically mixed.  
448 These results are consistent with the results in section 3.3 that the less reactive AVOCs  
449 and OVOCs are the dominant species in regulating the photochemical formation of  
450 ozone in urban regions aloft.

451 According to the vertical distribution patterns of the photochemical ozone  
452 formation regime, P(O<sub>3</sub>) decreases with increasing height alongside simultaneous



453 declines in concentrations of both NO<sub>x</sub> and VOCs. Fig. 8C presents the average diurnal  
454 and vertical variations in  $P(\text{O}_3)$  calculated by the box model during the campaign. The  
455  $P(\text{O}_3)$  values were higher in daytime and correlated well with  $j(\text{NO}_2)$ . As shown in Fig.  
456 S7, OH radical concentrations and  $P(\text{O}_3)$  exhibited contrasting vertical distribution  
457 patterns in daytime.  $P(\text{O}_3)$  decreased from the ground to 320 m, where it still maintained  
458 a relatively high value of approximately 10 ppb h<sup>-1</sup> at noon. These results highlight that  
459 the photochemical formation of ozone aloft also remained strong compared to those at  
460 ground level. Consequently, the downward transport of ozone from high altitudes,  
461 driven by turbulence mixing, can become significant sources of surface ozone during  
462 the day (Karl *et al.*, 2023).

463 Due to the measurement height limitation, the vertical distributions of  $P(\text{O}_3)$  in the  
464 middle and upper parts of the PBL were not determined in this study. As reported by  
465 the work in (Benish *et al.*, 2020),  $P(\text{O}_3)$  typically exhibited weak and nearly linear  
466 decline tendencies from 300 m to the top of the PBL during daytime.  $P(\text{O}_3)$  at the PBL  
467 top was approximately half of that at 300 m. Consequently, we can assume that  $P(\text{O}_3)$   
468 decreased linearly from 320 m to the top of the PBL. The integral of  $P(\text{O}_3)$  at different  
469 heights within the PBL can then be estimated using a similar method as described in  
470 Eq. (5).

471 As shown in Fig. 8D, the total amount of ozone photochemically produced below  
472 47 m constituted a mere 6% of the entire PBL. This fractional contribution increased to  
473 approximately 35% at 320 m, further corroborating that the majority of the boundary-  
474 layer ozone was produced in the middle and upper layers. Given the enhancement of  
475 turbulence vertical mixing in daytime, ozone produced at high altitudes becomes a  
476 significant source of surface ozone. This is substantiated by the widespread reports of  
477 strong downward ozone fluxes in the bottom part of the PBL (tens of meters above  
478 ground level) (Fares *et al.*, 2010; Liu *et al.*, 2021; Karl *et al.*, 2023). Consequently,  
479 when devising ozone control strategies, particularly in urban regions with intricate  
480 precursor emissions, careful considerations should be given to the vertical variations in  
481 the formation regimes of ozone in the PBL.



## 482 **4 Conclusions**

483 In this study, we investigated the vertical variations, key drivers, and  
484 environmental impacts of VOCs in the PBL using tower-based online gradient  
485 measurements in urban Beijing during the summer of 2021. The diurnal and vertical  
486 variations of various VOC species were strictly regulated by the diurnal evolution of  
487 the PBL. In daytime, reactive NMHC species were rapidly oxidized when they were  
488 mixed upward along with the formation of OVOCs. As a result, OVOC species played  
489 more significant roles in regulating the photochemical ozone formation in urban regions  
490 aloft. The photochemical formation of ozone belongs to the transition regime in the  
491 lower part of the PBL and becomes more sensitive to changes in the concentrations of  
492 AVOCs and OVOCs with increasing height.  $P(O_3)$  exhibited decreasing tendencies  
493 with height but remained very large in high altitudes, likely driven by the high  
494 concentrations of OVOCs and OH radicals. Therefore, careful consideration should be  
495 given to the vertical variations in both  $P(O_3)$  and photochemical ozone formation  
496 regimes in the whole PBL when making regional ozone control strategies.

497 The vertical variations in concentrations and compositions of VOCs significantly  
498 influence the formation of secondary pollutants. Furthermore, vertical changes in  
499 chemical reaction environments (e.g., temperature, humidity, and solar radiation) and  
500 concentrations of other chemicals (e.g., particulate matters, NO<sub>x</sub>, ozone) can also  
501 impact the degradation pathways of VOCs. These factors also affect the formation  
502 pathways and production yields of secondary pollutants. This is particularly crucial for  
503 the highly reactive NMHCs in urban areas with complex anthropogenic emissions and  
504 is expected to be thoroughly elucidated in future studies.

## 505 **Data availability**

506 The observational data used in this study are available from corresponding authors  
507 upon request.



## 508 **Author contributions**

509 BY, XBL, and YH designed the research. XBL, BY, YH, XS, JQ, XH, SW, YC,  
510 QY, YS, YP, GT, JG, and MS contributed to the data collection and data analysis. XBL,  
511 SY, and BY designed and performed the box model simulations. XBL and BY wrote  
512 the paper with contributions from all coauthors. All the coauthors discussed the results  
513 and reviewed the paper.

## 514 **Competing interests**

515 The authors declare that they have no conflict of interest.

## 516 **Acknowledgments**

517 The authors would like to thank the personnel who participated in data collection,  
518 instrument maintenance, and logistic support during the field campaign.

## 519 **Financial support**

520 This work was financially supported by the National Key R&D Plan of China  
521 (grant nos. 2023YFC3706103, 2023YFC3706201, 2023YFC3710900, and  
522 2022YFC3700604) and the National Natural Science Foundation of China (grant nos.  
523 42121004, 42275103, 42205094, 42230701, and 42305095, 42475107). This work was  
524 also supported by the Special Fund Project for Science and Technology Innovation  
525 Strategy of Guangdong Province (grant no. 2019B121205004), Guangdong Basic and  
526 Applied Basic Research Foundation (grant no. 2024A1515011570) and Guangzhou  
527 Basic and Applied Basic Research Foundation (grant no. 2024A04J3958).

## 528 **References**

529 An, J., Huang, Y., Huang, C., Wang, X., Yan, R., Wang, Q., Wang, H., Jing, S., Zhang,  
530 Y., Liu, Y., Chen, Y., Xu, C., Qiao, L., Zhou, M., Zhu, S., Hu, Q., Lu, J., and Chen, C.:  
531 Emission inventory of air pollutants and chemical speciation for specific anthropogenic  
532 sources based on local measurements in the Yangtze River Delta region, China, Atmos.  
533 Chem. Phys., 21, 2003-2025, <https://doi.org/10.5194/acp-21-2003-2021> 2021.



- 534 Atkinson, R., and Arey, J.: Atmospheric Degradation of Volatile Organic Compounds,  
535 Chem Rev, 103, 4605-4638,<https://doi.org/10.1021/cr0206420> 2003.
- 536 Benish, S. E., He, H., Ren, X., Roberts, S. J., Salawitch, R. J., Li, Z., Wang, F., Wang,  
537 Y., Zhang, F., Shao, M., Lu, S., and Dickerson, R. R.: Measurement report: Aircraft  
538 observations of ozone, nitrogen oxides, and volatile organic compounds over Hebei  
539 Province, China, Atmos. Chem. Phys., 20, 14523-14545,[https://doi.org/10.5194/acp-](https://doi.org/10.5194/acp-20-14523-2020)  
540 [20-14523-2020](https://doi.org/10.5194/acp-20-14523-2020) 2020.
- 541 Brown, S. S., Dubé, W. P., Osthoff, H. D., Wolfe, D. E., Angevine, W. M., and  
542 Ravishankara, A. R.: High resolution vertical distributions of NO<sub>3</sub> and N<sub>2</sub>O<sub>5</sub> through  
543 the nocturnal boundary layer, Atmos. Chem. Phys., 7, 139-149,[10.5194/acp-7-139-](https://doi.org/10.5194/acp-7-139-2007)  
544 [2007](https://doi.org/10.5194/acp-7-139-2007) 2007.
- 545 Cooper, O. R., Schultz, M. G., Schroeder, S., Chang, K.-L., Gaudel, A., Benitez, G. C.,  
546 Cuevas, E., Froehlich, M., Galbally, I. E., Molloy, S., Kubistin, D., Lu, X., McClure-  
547 Begley, A., Nedelec, P., O'Brien, J., Oltmans, S. J., Petropavlovskikh, I., Ries, L., Senik,  
548 I., Sjoeborg, K., Solberg, S., Spain, G. T., Spangl, W., Steinbacher, M., Tarasick, D.,  
549 Thouret, V., and Xu, X.: Multi-decadal surface ozone trends at globally distributed  
550 remote locations, Elementa-Science of the Anthropocene,  
551 8,<https://doi.org/10.1525/elementa.420> 2020.
- 552 Dieu Hien, V. T., Lin, C., Thanh, V. C., Kim Oanh, N. T., Thanh, B. X., Weng, C.-E.,  
553 Yuan, C.-S., and Rene, E. R.: An overview of the development of vertical sampling  
554 technologies for ambient volatile organic compounds (VOCs), J Environ Manage, 247,  
555 401-412,<https://doi.org/10.1016/j.jenvman.2019.06.090> 2019.
- 556 Fares, S., McKay, M., Holzinger, R., and Goldstein, A. H.: Ozone fluxes in a Pinus  
557 ponderosa ecosystem are dominated by non-stomatal processes: Evidence from long-  
558 term continuous measurements, Agr Forest Meteorol, 150, 420-  
559 431,<https://doi.org/10.1016/j.agrformet.2010.01.007> 2010.
- 560 Fleming, Z. L., Doherty, R. M., von Schneidmesser, E., Malley, C. S., Cooper, O. R.,  
561 Pinto, J. P., Colette, A., Xu, X., Simpson, D., Schultz, M. G., Lefohn, A. S., Hamad, S.,  
562 Moolla, R., Solberg, S., and Feng, Z.: Tropospheric Ozone Assessment Report: Present-  
563 day ozone distribution and trends relevant to human health, Elementa-Science of the  
564 Anthropocene, 6,[10.1525/elementa.273](https://doi.org/10.1525/elementa.273) 2018.
- 565 Geng, C., Wang, J., Yin, B., Zhao, R., Li, P., Yang, W., Xiao, Z., Li, S., Li, K., and Bai,  
566 Z.: Vertical distribution of volatile organic compounds conducted by tethered balloon  
567 in the Beijing-Tianjin-Hebei region of China, Journal of Environmental Sciences, 95,  
568 121-129,<https://doi.org/10.1016/j.jes.2020.03.026> 2020.
- 569 Geyer, A., and Stutz, J.: Vertical profiles of NO<sub>3</sub>, N<sub>2</sub>O<sub>5</sub>, O<sub>3</sub>, and NO<sub>x</sub> in the nocturnal  
570 boundary layer: 2. Model studies on the altitude dependence of composition and  
571 chemistry, Journal of Geophysical Research: Atmospheres,  
572 109,<https://doi.org/10.1029/2003jd004211> 2004.
- 573 Gkatzelis, G. I., Coggon, M. M., McDonald, B. C., Peischl, J., Gilman, J. B., Aikin, K.  
574 C., Robinson, M. A., Canonaco, F., Prevot, A. S. H., Trainer, M., and Warneke, C.:  
575 Observations Confirm that Volatile Chemical Products Are a Major Source of  
576 Petrochemical Emissions in U.S. Cities, Environ Sci Technol, 55, 4332-  
577 4343,[10.1021/acs.est.0c05471](https://doi.org/10.1021/acs.est.0c05471) 2021.



- 578 Gómez, M. C., Durana, N., García, J. A., de Blas, M., Sáez de Cámara, E., García-Ruiz,  
579 E., Gangoiti, G., Torre-Pascual, E., and Iza, J.: Long-term measurement of biogenic  
580 volatile organic compounds in a rural background area: Contribution to ozone  
581 formation, *Atmos Environ*, 224,  
582 117315,<https://doi.org/10.1016/j.atmosenv.2020.117315> 2020.
- 583 Guo, H., Ling, Z. H., Cheng, H. R., Simpson, I. J., Lyu, X. P., Wang, X. M., Shao, M.,  
584 Lu, H. X., Ayoko, G., Zhang, Y. L., Saunders, S. M., Lam, S. H. M., Wang, J. L., and  
585 Blake, D. R.: Tropospheric volatile organic compounds in China, *Sci Total Environ*,  
586 574, 1021-1043,<https://doi.org/10.1016/j.scitotenv.2016.09.116> 2017.
- 587 Guo, J.-X., Zeng, Y., Zhu, K., and Tan, X.: Vehicle mix evaluation in Beijing's  
588 passenger-car sector: From air pollution control perspective, *Sci Total Environ*, 785,  
589 147264,<https://doi.org/10.1016/j.scitotenv.2021.147264> 2021.
- 590 He, G., He, C., Wang, H., Lu, X., Pei, C., Qiu, X., Liu, C., Wang, Y., Liu, N., Zhang,  
591 J., Lei, L., Liu, Y., Wang, H., Deng, T., Fan, Q., and Fan, S.: Nighttime ozone in the  
592 lower boundary layer: insights from 3-year tower-based measurements in South China  
593 and regional air quality modeling, *Atmos. Chem. Phys.*, 23, 13107-13124,[10.5194/acp-](https://doi.org/10.5194/acp-23-13107-2023)  
594 23-13107-2023 2023.
- 595 He, X., Yuan, B., Wu, C., Wang, S., Wang, C., Huangfu, Y., Qi, J., Ma, N., Xu, W.,  
596 Wang, M., Chen, W., Su, H., Cheng, Y., and Shao, M.: Volatile organic compounds in  
597 wintertime North China Plain: Insights from measurements of proton transfer reaction  
598 time-of-flight mass spectrometer (PTR-ToF-MS), *J Environ Sci (China)*, 114, 98-  
599 114,[10.1016/j.jes.2021.08.010](https://doi.org/10.1016/j.jes.2021.08.010) 2022.
- 600 Hofzumahaus, A., Rohrer, F., Lu, K., Bohn, B., Brauers, T., Chang, C.-C., Fuchs, H.,  
601 Holland, F., Kita, K., Kondo, Y., Li, X., Lou, S., Shao, M., Zeng, L., Wahner, A., and  
602 Zhang, Y.: Amplified Trace Gas Removal in the Troposphere, *Science*, 324, 1702-  
603 1704,[doi:10.1126/science.1164566](https://doi.org/10.1126/science.1164566) 2009.
- 604 Karl, T., Lamprecht, C., Graus, M., Cede, A., Tiefengraber, M., Vila-Guerau de  
605 Arellano, J., Gurarie, D., and Lenschow, D.: High urban NO<sub>x</sub> triggers a substantial  
606 chemical downward flux of ozone, *Science Advances*, 9,  
607 eadd2365,[doi:10.1126/sciadv.add2365](https://doi.org/10.1126/sciadv.add2365) 2023.
- 608 Kaser, L., Patton, E. G., Pfister, G. G., Weinheimer, A. J., Montzka, D. D., Flocke, F.,  
609 Thompson, A. M., Stauffer, R. M., and Halliday, H. S.: The effect of entrainment  
610 through atmospheric boundary layer growth on observed and modeled surface ozone in  
611 the Colorado Front Range, *Journal of Geophysical Research: Atmospheres*, 122, 6075-  
612 6093,[10.1002/2016jd026245](https://doi.org/10.1002/2016jd026245) 2017.
- 613 Kim, S., Seco, R., Gu, D., Sanchez, D., Jeong, D., Guenther, A. B., Lee, Y., Mak, J. E.,  
614 Su, L., Kim, D. B., Lee, Y., Ahn, J.-Y., McGee, T., Sullivan, J., Long, R., Brune, W.  
615 H., Thames, A., Wisthaler, A., Mueller, M., Mikoviny, T., Weinheimer, A., Yang, M.,  
616 Woo, J.-H., Kim, S., and Park, H.: The role of a suburban forest in controlling vertical  
617 trace gas and OH reactivity distributions - a case study for the Seoul metropolitan area,  
618 *Faraday Discuss*, 226, 537-550,[10.1039/d0fd00081g](https://doi.org/10.1039/d0fd00081g) 2021.
- 619 Li, C., Liu, Y., Cheng, B., Zhang, Y., Liu, X., Qu, Y., An, J., Kong, L., Zhang, Y.,  
620 Zhang, C., Tan, Q., and Feng, M.: A comprehensive investigation on volatile organic  
621 compounds (VOCs) in 2018 in Beijing, China: Characteristics, sources and behaviours



622 in response to O<sub>3</sub> formation, *Sci Total Environ*, 806,  
623 150247, <https://doi.org/10.1016/j.scitotenv.2021.150247> 2022a.

624 Li, X.-B., Wang, D., Lu, Q.-C., Peng, Z.-R., Fu, Q., Hu, X.-M., Huo, J., Xiu, G., Li, B.,  
625 Li, C., Wang, D.-S., and Wang, H.: Three-dimensional analysis of ozone and PM<sub>2.5</sub>  
626 distributions obtained by observations of tethered balloon and unmanned aerial vehicle  
627 in Shanghai, China, *Stoch Env Res Risk A*, 32, 1189-  
628 1203, <https://doi.org/10.1007/s00477-018-1524-2> 2018.

629 Li, X.-B., and Fan, G.: Interannual variations, sources, and health impacts of the  
630 springtime ozone in Shanghai, *Environ Pollut*, 306,  
631 119458, <https://doi.org/10.1016/j.envpol.2022.119458> 2022.

632 Li, X.-B., Yuan, B., Parrish, D. D., Chen, D., Song, Y., Yang, S., Liu, Z., and Shao, M.:  
633 Long-term trend of ozone in southern China reveals future mitigation strategy for air  
634 pollution, *Atmos Environ*, 269, 118869, [10.1016/j.atmosenv.2021.118869](https://doi.org/10.1016/j.atmosenv.2021.118869) 2022b.

635 Li, X.-B., Yuan, B., Wang, S., Wang, C., Lan, J., Liu, Z., Song, Y., He, X., Huangfu,  
636 Y., Pei, C., Cheng, P., Yang, S., Qi, J., Wu, C., Huang, S., You, Y., Chang, M., Zheng,  
637 H., Yang, W., Wang, X., and Shao, M.: Variations and sources of volatile organic  
638 compounds (VOCs) in urban region: insights from measurements on a tall tower,  
639 *Atmos. Chem. Phys.*, 22, 10567-10587, [10.5194/acp-22-10567-2022](https://doi.org/10.5194/acp-22-10567-2022) 2022c.

640 Li, X.-B., Zhang, C., Liu, A., Yuan, B., Yang, H., Liu, C., Wang, S., Huangfu, Y., Qi,  
641 J., Liu, Z., He, X., Song, X., Chen, Y., Peng, Y., Zhang, X., Zheng, E., Yang, L., Yang,  
642 Q., Qin, G., Zhou, J., and Shao, M.: Assessment of long tubing in measuring  
643 atmospheric trace gases: applications on tall towers, *Environmental Science:  
644 Atmospheres*, 3, 506-520, [10.1039/d2ea00110a](https://doi.org/10.1039/d2ea00110a) 2023.

645 Li, X., Wang, W., Yang, S., Cheng, Y., Zeng, L., Yu, X., Lu, S., Liu, Y., Hu, M., Xie,  
646 S., Huang, X., Zhou, J., Shi, L., Xu, H., Lin, S., Liu, H., Feng, M., Song, D., Tan, Q.,  
647 and Zhang, Y.: Ozone sensitivity regimes vary at different heights in the planetary  
648 boundary layer, *Sci Total Environ*, 944,  
649 173712, <https://doi.org/10.1016/j.scitotenv.2024.173712> 2024.

650 Liu, X., Deming, B., Pagonis, D., Day, D. A., Palm, B. B., Talukdar, R., Roberts, J. M.,  
651 Veres, P. R., Krechmer, J. E., Thornton, J. A., de Gouw, J. A., Ziemann, P. J., and  
652 Jimenez, J. L.: Effects of gas-wall interactions on measurements of semivolatile  
653 compounds and small polar molecules, *Atmos. Meas. Tech.*, 12, 3137-  
654 3149, [10.5194/amt-12-3137-2019](https://doi.org/10.5194/amt-12-3137-2019) 2019.

655 Liu, Y., Tang, G., Wang, Y., Cheng, M., Gao, J., and Wang, Y.: Spatiotemporal  
656 differences in tropospheric ozone sensitivity and the impact of “dual carbon” goal,  
657 *Science Bulletin*, 69, 422-425, <https://doi.org/10.1016/j.scib.2023.12.026> 2024a.

658 Liu, Y., Yin, S., Zhang, S., Ma, W., Zhang, X., Qiu, P., Li, C., Wang, G., Hou, D.,  
659 Zhang, X., An, J., Sun, Y., Li, J., Zhang, Z., Chen, J., Tian, H., Liu, X., and Liu, L.:  
660 Drivers and impacts of decreasing concentrations of atmospheric volatile organic  
661 compounds (VOCs) in Beijing during 2016–2020, *Sci Total Environ*, 906,  
662 167847, <https://doi.org/10.1016/j.scitotenv.2023.167847> 2024b.

663 Liu, Z., Pan, Y., Song, T., Hu, B., Wang, L., and Wang, Y.: Eddy covariance  
664 measurements of ozone flux above and below a southern subtropical forest canopy, *Sci  
665 Total Environ*, 791, 148338, <https://doi.org/10.1016/j.scitotenv.2021.148338> 2021.



- 666 Lu, K. D., Rohrer, F., Holland, F., Fuchs, H., Bohn, B., Brauers, T., Chang, C. C.,  
667 Häseler, R., Hu, M., Kita, K., Kondo, Y., Li, X., Lou, S. R., Nehr, S., Shao, M., Zeng,  
668 L. M., Wahner, A., Zhang, Y. H., and Hofzumahaus, A.: Observation and modelling of  
669 OH and HO<sub>2</sub> concentrations in the Pearl River Delta 2006: a missing OH source in a  
670 VOC rich atmosphere, *Atmos. Chem. Phys.*, 12, 1541-1569, [10.5194/acp-12-1541-2012](https://doi.org/10.5194/acp-12-1541-2012)  
671 2012.
- 672 Lu, Y., Pang, X., Lyu, Y., Li, J., Xing, B., Chen, J., Mao, Y., Shang, Q., and Wu, H.:  
673 Characteristics and sources analysis of ambient volatile organic compounds in a typical  
674 industrial park: Implications for ozone formation in 2022 Asian Games, *Sci Total*  
675 *Environ*, 848, 157746, <https://doi.org/10.1016/j.scitotenv.2022.157746> 2022.
- 676 Ma, Z., Xu, H., Meng, W., Zhang, X., Xu, J., Liu, Q., and Wang, Y.: Vertical ozone  
677 characteristics in urban boundary layer in Beijing, *Environ Monit Assess*, 185, 5449-  
678 5460, [10.1007/s10661-012-2958-5](https://doi.org/10.1007/s10661-012-2958-5) 2013.
- 679 Mo, Z., Shao, M., Wang, W., Liu, Y., Wang, M., and Lu, S.: Evaluation of biogenic  
680 isoprene emissions and their contribution to ozone formation by ground-based  
681 measurements in Beijing, China, *Sci Total Environ*, 627, 1485-  
682 1494, <https://doi.org/10.1016/j.scitotenv.2018.01.336> 2018.
- 683 Mo, Z., Huang, S., Yuan, B., Pei, C., Song, Q., Qi, J., Wang, M., Wang, B., Wang, C.,  
684 Li, M., Zhang, Q., and Shao, M.: Deriving emission fluxes of volatile organic  
685 compounds from tower observation in the Pearl River Delta, China, *Sci Total Environ*,  
686 741, 139763, <https://doi.org/10.1016/j.scitotenv.2020.139763> 2020.
- 687 Niu, H., Li, K., Chu, B., Su, W., and Li, J.: Heterogeneous Reactions between Toluene  
688 and NO<sub>2</sub> on Mineral Particles under Simulated Atmospheric Conditions, *Environ Sci*  
689 *Technol*, 51, 9596-9604, <https://doi.org/10.1021/acs.est.7b00194> 2017.
- 690 Ou, J., Zheng, J., Li, R., Huang, X., Zhong, Z., Zhong, L., and Lin, H.: Speciated OVOC  
691 and VOC emission inventories and their implications for reactivity-based ozone control  
692 strategy in the Pearl River Delta region, China, *Sci Total Environ*, 530-531, 393-  
693 402, <https://doi.org/10.1016/j.scitotenv.2015.05.062> 2015.
- 694 Ou, J., Yuan, Z., Zheng, J., Huang, Z., Shao, M., Li, Z., Huang, X., Guo, H., and Louie,  
695 P. K. K.: Ambient Ozone Control in a Photochemically Active Region: Short-Term  
696 Despiking or Long-Term Attainment?, *Environ Sci Technol*, 50, 5720-  
697 5728, <https://doi.org/10.1021/acs.est.6b00345> 2016.
- 698 Pagonis, D., Krechmer, J. E., de Gouw, J., Jimenez, J. L., and Ziemann, P. J.: Effects  
699 of gas-wall partitioning in Teflon tubing and instrumentation on time-resolved  
700 measurements of gas-phase organic compounds, *Atmos. Meas. Tech.*, 10, 4687-  
701 4696, [10.5194/amt-10-4687-2017](https://doi.org/10.5194/amt-10-4687-2017) 2017.
- 702 Perdignes, B. C., Lee, S., Cohen, R. C., Park, J.-H., and Min, K.-E.: Two Decades of  
703 Changes in Summertime Ozone Production in California's South Coast Air Basin,  
704 *Environ Sci Technol*, 56, 10586-10595, [10.1021/acs.est.2c01026](https://doi.org/10.1021/acs.est.2c01026) 2022.
- 705 Qi, J., Mo, Z., Yuan, B., Huang, S., Huangfu, Y., Wang, Z., Li, X., Yang, S., Wang,  
706 W., Zhao, Y., Wang, X., Wang, W., Liu, K., and Shao, M.: An observation approach in  
707 evaluation of ozone production to precursor changes during the COVID-19 lockdown,  
708 *Atmos Environ*, 262, 118618, <https://doi.org/10.1016/j.atmosenv.2021.118618> 2021.





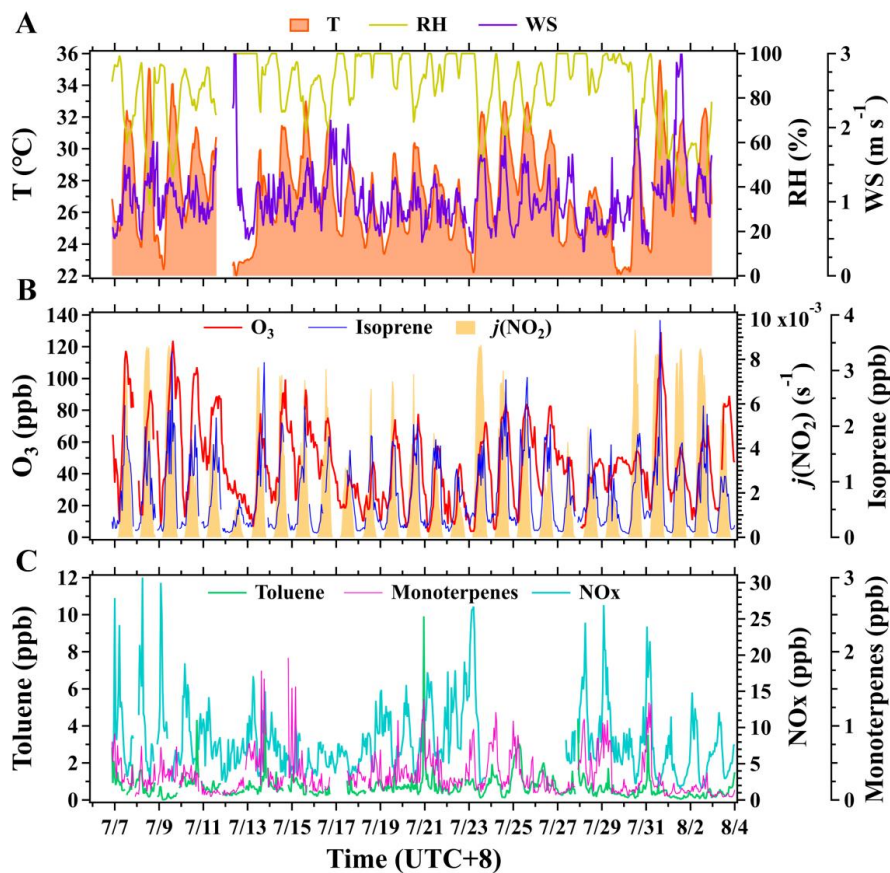
- 709 Sangiorgi, G., Ferrero, L., Perrone, M. G., Bolzacchini, E., Duane, M., and Larsen, B.  
710 R.: Vertical distribution of hydrocarbons in the low troposphere below and above the  
711 mixing height: Tethered balloon measurements in Milan, Italy, *Environ Pollut*, 159,  
712 3545-3552, <https://doi.org/10.1016/j.envpol.2011.08.012> 2011.
- 713 Shao, M., Wang, W., Yuan, B., Parrish, D. D., Li, X., Lu, K., Wu, L., Wang, X., Mo,  
714 Z., Yang, S., Peng, Y., Kuang, Y., Chen, W., Hu, M., Zeng, L., Su, H., Cheng, Y.,  
715 Zheng, J., and Zhang, Y.: Quantifying the role of PM<sub>2.5</sub> dropping in variations of  
716 ground-level ozone: Inter-comparison between Beijing and Los Angeles, *Sci Total*  
717 *Environ*, 147712, <https://doi.org/10.1016/j.scitotenv.2021.147712> 2021.
- 718 Souri, A. H., Nowlan, C. R., Wolfe, G. M., Lamsal, L. N., Chan Miller, C. E., Abad, G.  
719 G., Janz, S. J., Fried, A., Blake, D. R., Weinheimer, A. J., Diskin, G. S., Liu, X., and  
720 Chance, K.: Revisiting the effectiveness of HCHO/NO<sub>2</sub> ratios for inferring ozone  
721 sensitivity to its precursors using high resolution airborne remote sensing observations  
722 in a high ozone episode during the KORUS-AQ campaign, *Atmos Environ*, 224,  
723 117341, <https://doi.org/10.1016/j.atmosenv.2020.117341> 2020.
- 724 Sun, J., Wang, Y., Wu, F., Tang, G., Wang, L., Wang, Y., and Yang, Y.: Vertical  
725 characteristics of VOCs in the lower troposphere over the North China Plain during  
726 pollution periods, *Environ Pollut*, 236, 907-  
727 915, <https://doi.org/10.1016/j.envpol.2017.10.051> 2018.
- 728 Tang, G., Zhu, X., Xin, J., Hu, B., Song, T., Sun, Y., Zhang, J., Wang, L., Cheng, M.,  
729 Chao, N., Kong, L., Li, X., and Wang, Y.: Modelling study of boundary-layer ozone  
730 over northern China - Part I: Ozone budget in summer, *Atmos Res*, 187, 128-  
731 137, <https://doi.org/10.1016/j.atmosres.2016.10.017> 2017.
- 732 Velasco, E., Marquez, C., Bueno, E., Bernabe, R. M., Sanchez, A., Fentanes, O.,  
733 Wohrschimmel, H., Cardenas, B., Kamilla, A., Wakamatsu, S., and Molina, L. T.:  
734 Vertical distribution of ozone and VOCs in the low boundary layer of Mexico City,  
735 *Atmos. Chem. Phys.*, 8, 3061-3079, <https://doi.org/10.5194/acp-8-3061-2008> 2008.
- 736 Vo, T.-D.-H., Lin, C., Weng, C.-E., Yuan, C.-S., Lee, C.-W., Hung, C.-H., Bui, X.-T.,  
737 Lo, K.-C., and Lin, J.-X.: Vertical stratification of volatile organic compounds and their  
738 photochemical product formation potential in an industrial urban area, *J Environ*  
739 *Manage*, 217, 327-336, <https://doi.org/10.1016/j.jenvman.2018.03.101> 2018.
- 740 Wang, C., Yuan, B., Wu, C., Wang, S., Qi, J., Wang, B., Wang, Z., Hu, W., Chen, W.,  
741 Ye, C., Wang, W., Sun, Y., Wang, C., Huang, S., Song, W., Wang, X., Yang, S., Zhang,  
742 S., Xu, W., Ma, N., Zhang, Z., Jiang, B., Su, H., Cheng, Y., Wang, X., and Shao, M.:  
743 Measurements of higher alkanes using NO<sup>+</sup> chemical ionization in PTR-ToF-MS:  
744 important contributions of higher alkanes to secondary organic aerosols in China,  
745 *Atmos. Chem. Phys.*, 20, 14123-14138, <https://doi.org/10.5194/acp-20-14123-2020>  
746 2020a.
- 747 Wang, H., Ma, X., Tan, Z., Wang, H., Chen, X., Chen, S., Gao, Y., Liu, Y., Liu, Y.,  
748 Yang, X., Yuan, B., Zeng, L., Huang, C., Lu, K., and Zhang, Y.: Anthropogenic  
749 monoterpenes aggravating ozone pollution, *Natl Sci Rev*, 9,  
750 nwac103,10.1093/nsr/nwac103 2022a.



- 751 Wang, N., Lyu, X., Deng, X., Huang, X., Jiang, F., and Ding, A.: Aggravating O<sub>3</sub>  
752 pollution due to NO<sub>x</sub> emission control in eastern China, *Sci Total Environ*, 677, 732-  
753 744, <https://doi.org/10.1016/j.scitotenv.2019.04.388> 2019.
- 754 Wang, N., Huang, X., Xu, J., Wang, T., Tan, Z.-m., and Ding, A.: Typhoon-boosted  
755 biogenic emission aggravates cross-regional ozone pollution in China, *Science*  
756 *Advances*, 8, eabl6166, doi:10.1126/sciadv.abl6166 2022b.
- 757 Wang, W., Qi, J., Zhou, J., Yuan, B., Peng, Y., Wang, S., Yang, S., Williams, J., Sinha,  
758 V., and Shao, M.: The improved comparative reactivity method (ICRM): measurements  
759 of OH reactivity under high-NO<sub>x</sub> conditions in ambient air, *Atmos. Meas. Tech.*, 14,  
760 2285-2298, 10.5194/amt-14-2285-2021 2021a.
- 761 Wang, W., Yuan, B., Peng, Y., Su, H., Cheng, Y., Yang, S., Wu, C., Qi, J., Bao, F.,  
762 Huangfu, Y., Wang, C., Ye, C., Wang, Z., Wang, B., Wang, X., Song, W., Hu, W.,  
763 Cheng, P., Zhu, M., Zheng, J., and Shao, M.: Direct observations indicate  
764 photodegradable oxygenated volatile organic compounds (OVOCs) as larger  
765 contributors to radicals and ozone production in the atmosphere, *Atmos. Chem. Phys.*,  
766 22, 4117-4128, 10.5194/acp-22-4117-2022 2022c.
- 767 Wang, W., Li, X., Cheng, Y., Parrish, D. D., Ni, R., Tan, Z., Liu, Y., Lu, S., Wu, Y.,  
768 Chen, S., Lu, K., Hu, M., Zeng, L., Shao, M., Huang, C., Tian, X., Leung, K. M., Chen,  
769 L., Fan, M., Zhang, Q., Rohrer, F., Wahner, A., Pöschl, U., Su, H., and Zhang, Y.:  
770 Ozone pollution mitigation strategy informed by long-term trends of atmospheric  
771 oxidation capacity, *Nature Geoscience*, 17, 20-25, 10.1038/s41561-023-01334-9 2024.
- 772 Wang, Y., Wang, Y., Tang, G., Yang, Y., Li, X., Yao, D., Wu, S., Kang, Y., Wang, M.,  
773 and Wang, Y.: High gaseous carbonyl concentrations in the upper boundary layer in  
774 Shijiazhuang, China, *Sci Total Environ*, 799,  
775 149438, <https://doi.org/10.1016/j.scitotenv.2021.149438> 2021b.
- 776 Wang, Y. H., Gao, W. K., Wang, S., Song, T., Gong, Z. Y., Ji, D. S., Wang, L. L., Liu,  
777 Z. R., Tang, G. Q., Huo, Y. F., Tian, S. L., Li, J. Y., Li, M. G., Yang, Y., Chu, B. W.,  
778 Petaja, T., Kerminen, V. M., He, H., Hao, J. M., Kulmala, M., Wang, Y. S., and Zhang,  
779 Y. H.: Contrasting trends of PM<sub>2.5</sub> and surface-ozone concentrations in China from  
780 2013 to 2017, *National Science Review*, 7, 1331-  
781 1339, <https://doi.org/10.1093/nsr/nwaa032> 2020b.
- 782 Wolfe, G. M., Marvin, M. R., Roberts, S. J., Travis, K. R., and Liao, J.: The Framework  
783 for 0-D Atmospheric Modeling (F0AM) v3.1, *Geoscientific Model Development*, 9,  
784 3309-3319, 10.5194/gmd-9-3309-2016 2016.
- 785 Wu, C., Wang, C., Wang, S., Wang, W., Yuan, B., Qi, J., Wang, B., Wang, H., Wang,  
786 C., Song, W., Wang, X., Hu, W., Lou, S., Ye, C., Peng, Y., Wang, Z., Huangfu, Y., Xie,  
787 Y., Zhu, M., Zheng, J., Wang, X., Jiang, B., Zhang, Z., and Shao, M.: Measurement  
788 report: Important contributions of oxygenated compounds to emissions and chemistry  
789 of volatile organic compounds in urban air, *Atmos. Chem. Phys.*, 20, 14769-  
790 14785, <https://doi.org/10.5194/acp-20-14769-2020> 2020.
- 791 Yang, Q., Li, X. B., Yuan, B., Zhang, X., Huangfu, Y., Yang, L., He, X., Qi, J., and  
792 Shao, M.: Measurement report: Enhanced photochemical formation of formic and  
793 isocyanic acids in urban regions aloft – insights from tower-based online gradient  
794 measurements, *Atmos. Chem. Phys.*, 24, 6865-6882, 10.5194/acp-24-6865-2024 2024a.

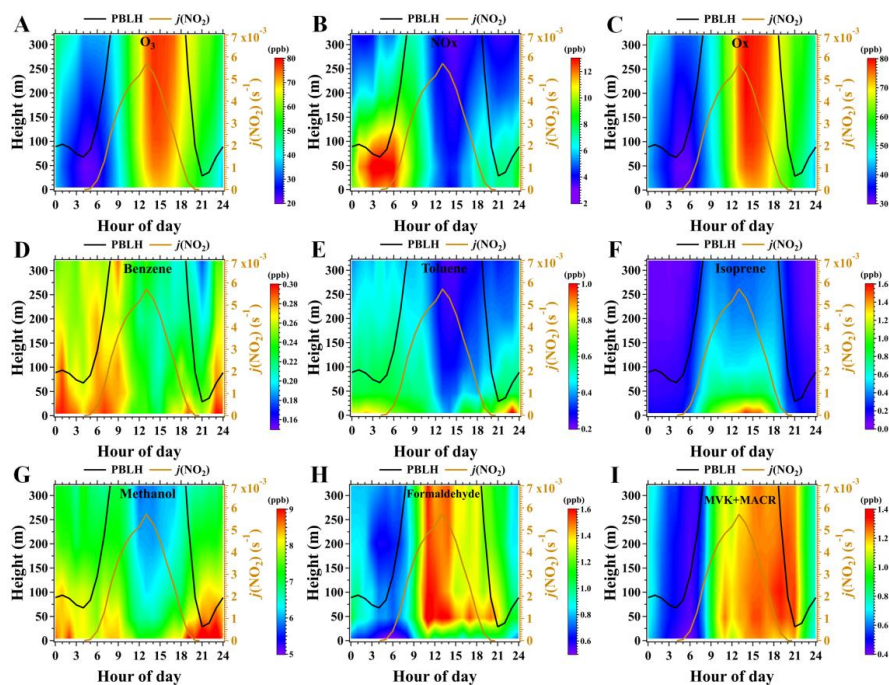


- 795 Yang, S., Yuan, B., Peng, Y., Huang, S., Chen, W., Hu, W., Pei, C., Zhou, J., Parrish,  
796 D. D., Wang, W., He, X., Cheng, C., Li, X. B., Yang, X., Song, Y., Wang, H., Qi, J.,  
797 Wang, B., Wang, C., Wang, C., Wang, Z., Li, T., Zheng, E., Wang, S., Wu, C., Cai, M.,  
798 Ye, C., Song, W., Cheng, P., Chen, D., Wang, X., Zhang, Z., Wang, X., Zheng, J., and  
799 Shao, M.: The formation and mitigation of nitrate pollution: comparison between urban  
800 and suburban environments, *Atmos. Chem. Phys.*, 22, 4539-4556, [10.5194/acp-22-](https://doi.org/10.5194/acp-22-4539-2022)  
801 [4539-2022](https://doi.org/10.5194/acp-22-4539-2022) 2022.
- 802 Yang, X., Wang, H., Lu, K., Ma, X., Tan, Z., Long, B., Chen, X., Li, C., Zhai, T., Li,  
803 Y., Qu, K., Xia, Y., Zhang, Y., Li, X., Chen, S., Dong, H., Zeng, L., and Zhang, Y.:  
804 Reactive aldehyde chemistry explains the missing source of hydroxyl radicals, *Nature*  
805 *Communications*, 15, 1648, [10.1038/s41467-024-45885-w](https://doi.org/10.1038/s41467-024-45885-w) 2024b.
- 806 Ye, C., Yuan, B., Lin, Y., Wang, Z., Hu, W., Li, T., Chen, W., Wu, C., Wang, C., Huang,  
807 S., Qi, J., Wang, B., Wang, C., Song, W., Wang, X., Zheng, E., Krechmer, J. E., Ye, P.,  
808 Zhang, Z., Wang, X., Worsnop, D. R., and Shao, M.: Chemical characterization of  
809 oxygenated organic compounds in the gas phase and particle phase using iodide CIMS  
810 with FIGAERO in urban air, *Atmos. Chem. Phys.*, 21, 8455-  
811 [8478, <https://doi.org/10.5194/acp-21-8455-2021>](https://doi.org/10.5194/acp-21-8455-2021) 2021.
- 812 Yeo, M. J., and Kim, Y. P.: Long-term trends of surface ozone in Korea, *Journal of*  
813 *Cleaner Production*, 294, 125352, <https://doi.org/10.1016/j.jclepro.2020.125352> 2021.
- 814 Yuan, B., Koss, A. R., Warneke, C., Coggon, M., Sekimoto, K., and de Gouw, J. A.:  
815 Proton-Transfer-Reaction Mass Spectrometry: Applications in Atmospheric Sciences,  
816 *Chem Rev*, 117, 13187-13229, <https://doi.org/10.1021/acs.chemrev.7b00325> 2017.
- 817 Zhang, K., Xiu, G., Zhou, L., Bian, Q., Duan, Y., Fei, D., Wang, D., and Fu, Q.: Vertical  
818 distribution of volatile organic compounds within the lower troposphere in late spring  
819 of Shanghai, *Atmos Environ*, 186, 150-  
820 [157, <https://doi.org/10.1016/j.atmosenv.2018.03.044>](https://doi.org/10.1016/j.atmosenv.2018.03.044) 2018.
- 821 Zhang, Y., Xue, L., Mu, J., Chen, T., Li, H., Gao, J., and Wang, W.: Developing the  
822 Maximum Incremental Reactivity for Volatile Organic Compounds in Major Cities of  
823 Central-Eastern China, *Journal of Geophysical Research: Atmospheres*, 127,  
824 [e2022JD037296, <https://doi.org/10.1029/2022JD037296>](https://doi.org/10.1029/2022JD037296) 2022.
- 825 Zhao, M., Zhang, Y., Pei, C., Chen, T., Mu, J., Liu, Y., Wang, Y., Wang, W., and Xue,  
826 L.: Worsening ozone air pollution with reduced NO<sub>x</sub> and VOCs in the Pearl River Delta  
827 region in autumn 2019: Implications for national control policy in China, *J Environ*  
828 *Manage*, 324, 116327, <https://doi.org/10.1016/j.jenvman.2022.116327> 2022.



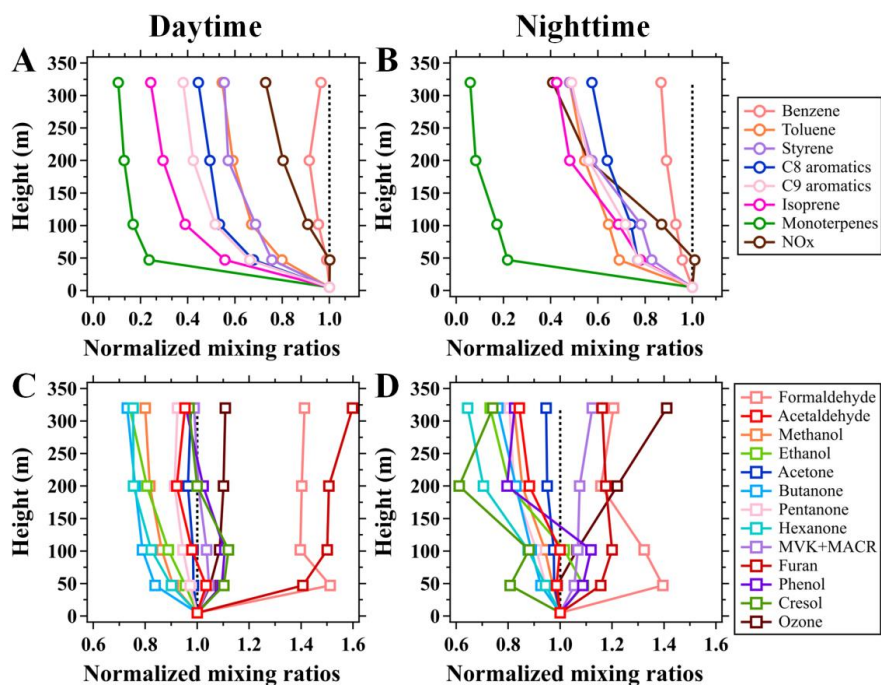
829

830 **Figure 1.** Time series of hourly mean air temperature (T), relative humidity (RH), wind  
 831 speed (WS), and mixing ratios of surface ozone, NO<sub>x</sub>, and VOC species along with  
 832 *j*(NO<sub>2</sub>) at the BMT site during the campaign. Meteorological parameters were measured  
 833 at 8 m above ground level and mixing ratios of ozone and its selected precursors were  
 834 measured at 5 m above ground level.



835

836 **Figure 2.** Average diurnal and vertical variations in mixing ratios ozone, NO<sub>x</sub>, Ox  
837 (O<sub>3</sub>+NO<sub>2</sub>), and six selected VOC species along with the average diurnal profiles of  
838 PBLH and  $j(\text{NO}_2)$  during the campaign. The figures were obtained by linearly  
839 interpolating the data at the five inlet heights on both altitude and temporal scales.



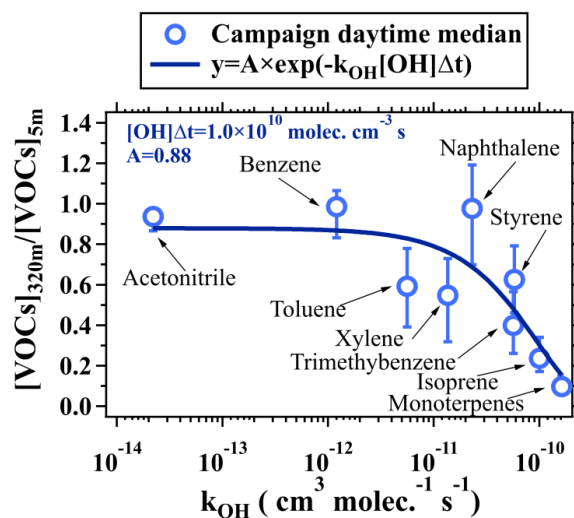
840

841 **Figure 3.** Average vertical profiles of (A-B) NMHCs and NO<sub>x</sub>, (C-D) OVOCs and O<sub>3</sub>

842 during the daytime (11:00-16:00 LT) and nighttime (23:00-04:00 LT) of the campaign.

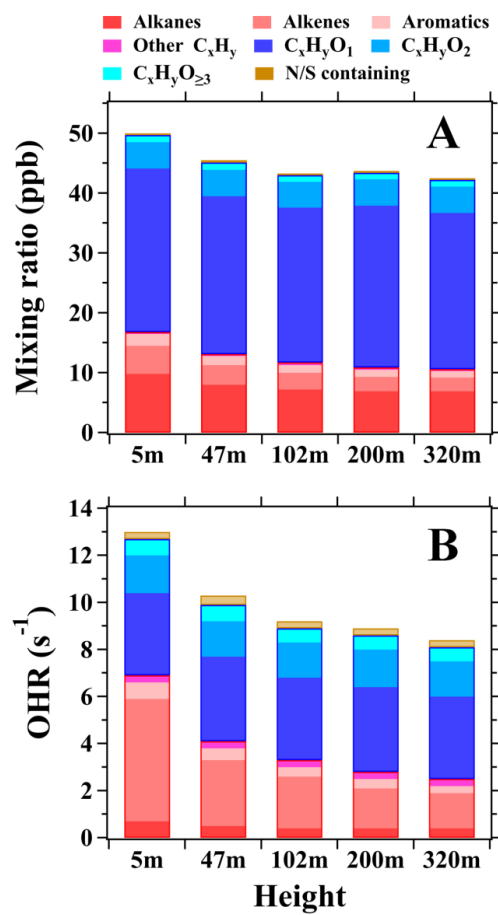
843 The mixing ratios of the chemical species measured above 5 m are normalized to those

844 at 5 m.



845

846 **Figure 4.** The change in ratios of NMHC concentrations (including acetonitrile)  
847 between 320 m and 5 m as a function of  $k_{OH}$ . The vertically-resolved measurements of  
848 VOCs made on the BMT in daytime during the campaign were used for analysis.  
849 Hollow markers represent median values and error bars indicate the range between 25<sup>th</sup>  
850 and 75<sup>th</sup> percentiles.

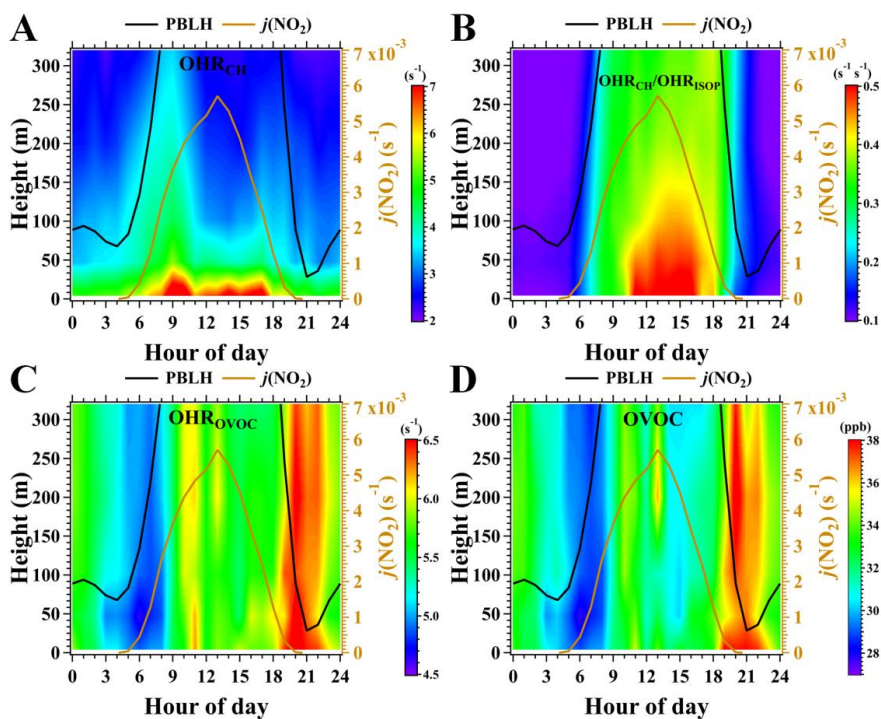


851

852 **Figure 5.** (A) Mean mixing ratios and (B) OHRs of different VOC categories at the five

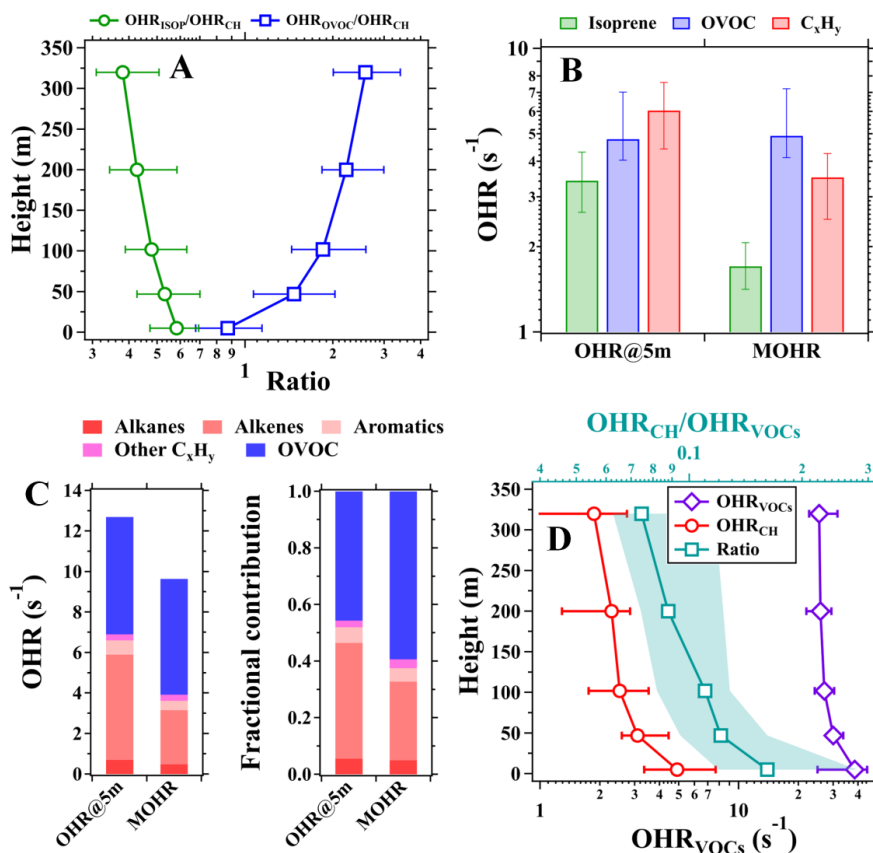
853 inlet heights in daytime during the campaign.





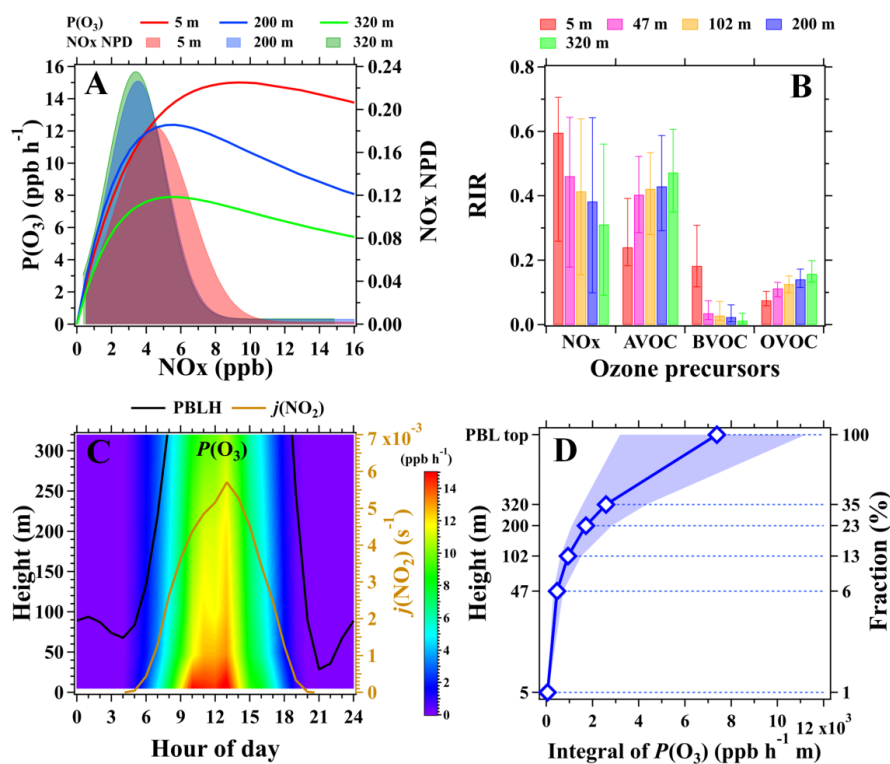
854

855 **Figure 6.** (A-B) Average diurnal and vertical variations in OHRs of  $\text{C}_x\text{H}_y$  and the OHR  
 856 ratios of isoprene to  $\text{C}_x\text{H}_y$  ( $\text{OHR}_{\text{ISOP}}/\text{OHR}_{\text{CH}}$ ) during the campaign. (C-D) Average  
 857 diurnal and vertical variations in mixing ratios and OHRs of OVOC. ISOP refers to  
 858 isoprene. The figures were obtained by linearly interpolating the data at the five  
 859 measurement heights on both altitude and temporal scales.



860

861 **Figure 7.** (A) Average vertical profiles of OHR ratios of isoprene to  $C_xH_y$   
 862 ( $OHR_{ISOP}/OHR_{CH}$ ) and OVOC to NMHC ( $OHR_{OVOC}/OHR_{CH}$ ). (B) Median values of  
 863 the OHR at 5 m and the mean OHR (MOHR) between 5 m and 320 m for isoprene,  
 864 OVOC, and  $C_xH_y$ . (C) Mean contributions of different VOC categories to the MOHR  
 865 below 320 m and the OHR at 5 m. (D) Vertical profiles of the measured  $OHR_{VOCs}$  and  
 866 the calculated  $OHR_{CH}$  (bottom axis) and the  $OHR_{CH}/OHR_{VOCs}$  ratios (top axis) during  
 867 July 28-31, 2021. The data used for analysis in panels A-D was within the time window  
 868 from 11:00 to 16:00 LT during the campaign. Markers in panels A and D represent  
 869 median values. Shaded areas and error bars in panels A, B, and D indicate the range  
 870 between 25<sup>th</sup> and 75<sup>th</sup> percentiles.



871

872 **Figure 8.** (A) Left axis: average dependence of  $P(O_3)$  on  $NO_x$  concentrations in  
 873 daytime during the campaign; Right axis: normalized probability density (NPD) of  
 874  $NO_x$  mixing ratios in daytime at the three inlet heights. (B) Median RIR values of  
 875 photochemical ozone formation to changes in  $NO_x$ , AVOC (NMHCs excluding BVOC),  
 876 BVOC (isoprene), and OVOC (nine OVOC species in Table S1) at the five inlet heights;  
 877 Error bars indicate the range between 25<sup>th</sup> and 75<sup>th</sup> percentiles. (C) Average diurnal and  
 878 vertical variations in  $P(O_3)$  during the campaign; The figure was obtained by linearly  
 879 interpolating the data at the five measurement heights on both altitude and temporal  
 880 scales. (D) The vertical profile of the integral of  $P(O_3)$  in daytime during the campaign;  
 881 Markers indicate median values and Shaded areas indicate the range between 25<sup>th</sup> and  
 882 75<sup>th</sup> percentiles.